NMR tomography of the three-qubit Deutsch-Jozsa algorithm

Oliver Mangold, Andreas Heidebrecht, and Michael Mehring*
2. Physikalisches Institut, University of Stuttgart, Stuttgart, Germany
(Received 7 June 2004; published 11 October 2004)

The optimized version of the Deutsch-Jozsa algorithm proposed by Collins *et al.* was implemented using the three ^{19}F nuclear spins of 2,3,4-trifluoroaniline as qubits. To emulate the behavior of pure quantum-mechanical states *pseudopure states* of the ensemble were prepared prior to execution of the algorithm. Full tomography of the density matrix was employed to obtain detailed information about initial, intermediate, and final states. Information, thus obtained, was applied to optimize the pulse sequences used. It is shown that substantial improvement of the fidelity of the preparation may be achieved by compensating the effects caused by the different relaxation behavior of the different substates of the density matrix. All manipulations of the quantum states were performed under the conditions of unresolved spin-spin interactions.

DOI: 10.1103/PhysRevA.70.042307 PACS number(s): 03.67.Lx, 03.67.Mn, 03.65.Wj

I. INTRODUCTION

Theoretical aspects of quantum information processing and, in particular, quantum computing have been published already extensively [1–13]. In contrast, only very few cases of experimental implementations have been reported, mostly with liquid-state NMR [14–25]. Besides the more recent demonstration of the two-qubit Deutsch-Jozsa (DJ) algorithm in an ion trap setup [26], already several years ago the two-qubit version of the DJ algorithm [16,19,21,27] and a little later the three-qubit Collins version of the DJ algorithm [28] were emulated by liquid-state NMR experiments [23].

The first implementation of the Collins version of the DJ algorithm was reported by Arvind *et al.* [23]. In this contribution, we extend their work by preparing all eight pseudopure initial density matrices $\rho_{000}-\rho_{111}$ to be used as input to the algorithm and performing a complete tomography of the input and output states of the different oracle functions.

Another major difference with respect to the implementation presented by Arvind is that we are dealing with a system of nonresolved spin-spin interactions. That is, there is no line splitting due to these interactions in the NMR spectrum and only spin-selective transitions can be excited. In contrast to the commonly reported liquid-state NMR quantum computing, this situation is more akin to the one found in solids. The implementation and tomography presented here will, therefore, also be applicable to other quantum computing scenarios where only qubit-selective manipulations are possible.

Compared to the conditions of nonresolved spin-spin interactions, high-resolution NMR spectra provide more information on the quantum-mechanical state of the system. However, whether spin couplings are resolved or not, most of the correlation terms of the density matrix are not available from simple spectra. More elaborate techniques are thus required. Therefore, we have used the full tomography of the 8×8 density matrices to obtain complete knowledge of the quantum-mechanical states of the spin system.

II. DEUTSCH-JOZSA ALGORITHM AND ITS OPTIMIZED VERSION

The Deutsch-Jozsa algorithm was one of the first quantum algorithms implemented with nuclear spins in liquid-state NMR [16,19,27]. In the following, we briefly summarize the concepts of the Deutsch-Jozsa algorithm.

A. Deutsch-Jozsa problem

The Deutsch-Jozsa problem [2] considers a set of functions which map a binary string of length N to a single bit:

$$f:\mathbb{Z}_{2^N}\mapsto\mathbb{Z}_2. \tag{1}$$

We are given an opaque physical device U_f (called an *oracle* for f) which when given an input i will produce the corresponding output $f(i)$ of an *a priori* unknown function f from the set defined in Eq. (1). The task consists of answering the question whether the function f has any of the two properties: (i) it is constant or (ii) it is balanced, meaning that applied to all possible inputs it outputs 0 exactly as often as 1. Deutsch and Jozsa have shown that, for a reasonable model of the oracle U_f, a quantum computer can solve this problem exponentially faster than a classical computer.

B. Optimized version of the Deutsch-Jozsa algorithm

The original version of the algorithm required $N+1$ qubits for a N-bit function and two applications of U_f. Later, Cleve, Ekert, Macchiavello, and Mosca (CEMM) modified the Deutsch-Jozsa algorithm by reducing the number of evaluations of U_f to one [29]. Collins, Kim, and Holton removed the requirement of an ancilla qubit [28]. We used this optimized version of the DJ algorithm for the work reported here.

*Electronic address: m.mehring@physik.uni-stuttgart.de; URL: http://www.physik.uni-stuttgart.de/ExPhys/2.Phys.Inst./MMgroup/index.html

 ©2004 The American Physical Society

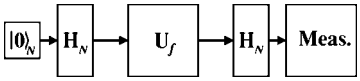

FIG. 1. Block diagram of the CEMM version of the Deutsch-Jozsa algorithm for N qubits.

The block diagram for this extended version of the algorithm is shown in Fig. 1. Here $|0\rangle_N$ is the initial state with all N qubits in state $|0\rangle$. The application of U_f is defined by

$$|0\rangle_N \xrightarrow{H_N} \frac{1}{\sqrt{2^N}} \sum_{k=0}^{2^N-1} |k\rangle_N \xrightarrow{U_f} \frac{1}{\sqrt{2^N}} \sum_{k=0}^{2^N-1} \times (-1)^{f(k)} |k\rangle_N \xrightarrow{H_N} \frac{1}{2^N} \sum_{k=0}^{2^N-1} (-1)^{f(k)} \sum_{m=0}^{2^N-1} (-1)^{\sum_{j=0}^{N-1} m_j k_j} |m\rangle_N. \tag{2}$$

$H_N = H \otimes H \otimes \cdots \otimes H \otimes H$ is the *Hadamard* transform applied to all N qubits simultaneously. The Hadamard transform of one qubit is defined by

$$H = \frac{1}{\sqrt{2}} \begin{pmatrix} 1 & 1 \\ 1 & -1 \end{pmatrix} \tag{3}$$

and is equal to its inverse. The decision on the class of the test function is based upon the amplitude of the state $|0\rangle_N$ in the output state:

$$P(|0\rangle_N) = \frac{1}{2^N} \left| \sum_{k=0}^{2^N-1} (-1)^{f(k)} \right| = \begin{cases} 1 & \text{if } f \text{ constant,} \\ 0 & \text{if } f \text{ balanced.} \end{cases} \tag{4}$$

III. EXPERIMENT

All manipulations were implemented using liquid-state NMR at 313 MHz. The compound used was pure 2,3,4-trifluoroaniline whose molecular structure and ^{19}F free induction decay (FID) spectrum are shown in Fig. 2. The chemical shifts and J couplings were obtained through a standard two-dimensional (2D) echo modulation experiment and are summarized in Table I. The coupling between spins 1

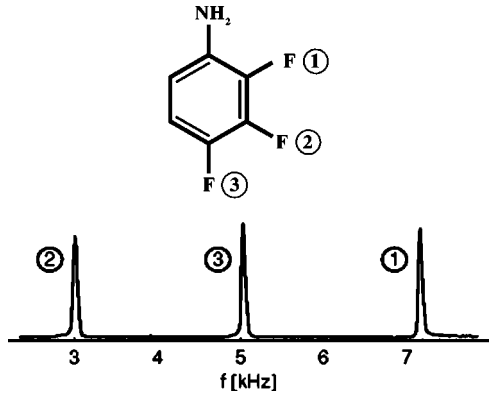

FIG. 2. Molecular structure and the spectrum of 2,3,4 trifluoroaniline.

TABLE I. Chemical shifts and J couplings of the ^{19}F in 2,3,4 trifluoroaniline. Chemical shifts are given relative to spin number 2. Note that the numbering of spins is different from the chemical nomenclature.

	2	3	1
2	0 ppm	20.0 Hz	19.3 Hz
3		6.48 ppm	1.5 Hz
1			13.28 ppm

and 3 is very weak compared to the next-neighbor couplings and all couplings are much smaller than the chemical shifts. In addition, $J_{12} \approx J_{23} \approx 20$ Hz. Thus, the following approximate Hamiltonian was used in all calculations:

$$\boldsymbol{H} = \omega_1 \mathbf{I}_{z_1} + \omega_2 \mathbf{I}_{z_2} + \omega_3 \mathbf{I}_{z_3} + 2\pi J(\mathbf{I}_{z_1}\mathbf{I}_{z_2} + \mathbf{I}_{z_2}\mathbf{I}_{z_3}). \tag{5}$$

Relaxation times of the three spins at room temperature differ slightly and lie in the range $T_1 = 3.3-4.7$ s, $T_2 = 200$ ms.

Selective excitation was achieved through soft rf pulses of 2 ms duration applied separately or simultaneously. To reduce undesired effects on neighboring spins, the pulses were given a Fermi-type envelope. Required rotation angles were adjusted by choosing proper rf-pulse amplitudes. Gradient pulses required for the preparation of pseudopure states were implemented by an additional coil parallel to the main field. Pulse lengths were on the same order of magnitude as those of the rf pulses. Instead of the Hadamard transform, we used $\pi/2$ pulses in the y direction and their inverses where appropriate. More details can be found in [30].

IV. PREPARATION AND TOMOGRAPHY OF PSEUDOPURE STATES

A. Notation

1. Density matrices

The density matrices for a system of three $I=1/2$ spins are Hermitian 8×8 matrices. The density matrices of the pure states of such a system have all elements equal to 0 except for one element on the main diagonal, which is equal to 1. E.g., the pure state ρ_{000} is given by

TABLE II. Parameters for the preparation sequence for the pseudopure states.

ρ	000	001	010	011	100	101	110	111
η	$\pi/3$	$\pi/3$	$\pi/3$	$\pi/3$	$2\pi/3$	$2\pi/3$	$\pi/3$	$\pi/3$
χ	$\pi/4$	$\pi/4$	$\pi/4$	$\pi/4$	$-3\pi/4$	$\pi/4$	$\pi/4$	$\pi/4$
ξ_1	0	0	0	0	0	0	π	π
ξ_2	π	π	0	0	π	π	0	0
ξ_3	$-3\pi/4$	$\pi/4$	$-3\pi/4$	$\pi/4$	$-3\pi/4$	$-3\pi/4$	$-3\pi/4$	$\pi/4$

$$\rho_{000} = \begin{pmatrix} 1 & 0 & 0 & 0 & 0 & 0 & 0 & 0 \\ 0 & 0 & 0 & 0 & 0 & 0 & 0 & 0 \\ 0 & 0 & 0 & 0 & 0 & 0 & 0 & 0 \\ 0 & 0 & 0 & 0 & 0 & 0 & 0 & 0 \\ 0 & 0 & 0 & 0 & 0 & 0 & 0 & 0 \\ 0 & 0 & 0 & 0 & 0 & 0 & 0 & 0 \\ 0 & 0 & 0 & 0 & 0 & 0 & 0 & 0 \\ 0 & 0 & 0 & 0 & 0 & 0 & 0 & 0 \end{pmatrix}. \quad (6)$$

For the purpose of discussion of NMR experiments, the density matrices are most conveniently expressed in the basis of the spin component operators:

$$\{\mathbf{I}_0, \mathbf{I}_{\alpha_i}, \mathbf{I}_{\alpha_i}\mathbf{I}_{\beta_j}, \mathbf{I}_{\alpha_i}\mathbf{I}_{\beta_j}\mathbf{I}_{\gamma_k}\}, \quad (7)$$

where $\mathbf{I}_0$ is the 8×8 identity matrix, $\alpha,\beta,\gamma \in \{x,y,z\}$ denote the spin components, and $i,j,k \in \{1,2,3\}$ the spin numbers. Product terms with multiple occurrences of the same spin component operator are excluded. The term $\mathbf{I}_{z_1}\mathbf{I}_{x_3}$, for instance, is constructed by taking the dyadic product $\mathbf{I}_{z_1}\mathbf{I}_{x_3} = \mathbf{I}_z \otimes \mathbf{I}_0 \otimes \mathbf{I}_x$ of the spin-1/2 matrices and the 2×2 identity matrix.

Using this basis, the pure state ρ_{000} can be written as

$$\rho_{000} = \tfrac{1}{8}\mathbf{I}_0 + \tfrac{1}{4}\mathbf{I}_{z_1} + \tfrac{1}{4}\mathbf{I}_{z_2} + \tfrac{1}{4}\mathbf{I}_{z_3} + \tfrac{1}{2}\mathbf{I}_{z_1}\mathbf{I}_{z_2} + \tfrac{1}{2}\mathbf{I}_{z_2}\mathbf{I}_{z_3} + \tfrac{1}{2}\mathbf{I}_{z_3}\mathbf{I}_{z_1} + \mathbf{I}_{z_1}\mathbf{I}_{z_2}\mathbf{I}_{z_3}. \quad (8)$$

The representation of the other pure states consists of the same terms with different sign combinations.

2. Pulse sequences

In the description of the pulse sequences the following shorthand notation is used.

(a) rf pulses:

$$P_{x_j}(\beta,\phi) = e^{-i\phi I_{zj}} e^{-i\beta I_{xj}} e^{i\phi I_{zj}} \quad (9)$$

special cases of which are

$$P_{x_j}(\beta) = P_{x_j}(\beta,0),$$

$$P_{-x_j}(\beta) = P_{x_j}(\beta,\pi),$$

$$P_{y_j}(\beta) = P_{x_j}(\beta,\pi/2),$$

$$P_{-y_j}(\beta) = P_{x_j}(\beta,-\pi/2).$$

(b) Gradient pulses:

$$G = \frac{1}{2\pi}\int_{\beta=0}^{2\pi} \mathrm{d}\beta\, P_{z_{1,2,3}}(\beta). \quad (10)$$

(c) free evolution under an arbitrary and time dependent Hamiltonian $\boldsymbol{H}$:

$$U(\tau) = T\exp\left(-i\int_0^\tau \mathrm{d}t\, \boldsymbol{H}(t)\right), \quad (11)$$

where T is the Dyson time ordering operator.

The unitary transformation of density matrices by pulse sequences are abbreviated by applying the Liouville notation as in the following [31].

(a) rf pulses:

$$P_{x_j}(\beta,\phi)|\rho) = P_{x_j}(\beta,\phi)\rho P_{x_j}(-\beta,\phi). \quad (12)$$

(b) Gradient pulses:

$$G\rho = \frac{1}{2\pi}\int_{\beta=0}^{2\pi} \mathrm{d}\beta\, P_{z_{1,2,3}}(\beta)\rho P_{z_{1,2,3}}(-\beta). \quad (13)$$

(c) Free evolution:

$$U(\tau)|\rho) = \left[T\exp\left(-i\int_0^\tau \mathrm{d}t\, \boldsymbol{H}(t)\right)\right]\rho\left[T \times \exp\left(i\int_0^\tau \mathrm{d}t\, \boldsymbol{H}(t)\right)\right]. \quad (14)$$

The pulses in a sequence are written from right to left in the order in which they are applied. Multiple spin numbers imply that the pulse is applied to several spins simultaneously as are successive commuting pulses.

B. Preparation

1. Sequence

The pulse sequence used for the preparation of the eight pseudopure states starting at the *Boltzmann state* may be written as

$$|\rho_{ijk}) = G\cdot P_{x_3}(\xi_3)\cdot P_{x_2}(\xi_2)\cdot P_{x_1}(\xi_1)\cdot U(\tau)\cdot P_{-x_{1,2,3}}(\pi)\cdot U(\tau)\cdot P_{y_1}(\chi)\cdot G\cdot P_{x_1}\left(\frac{3\pi}{4}\right)\cdot U(\tau)\cdot P_{-x_{1,2,3}}(\pi)\cdot U(\tau)\cdot P_{y_1}\left(\frac{\pi}{4}\right) \cdot G\cdot P_{y_2}(\beta_2)\cdot U(\tau)\cdot P_{-x1,2,3}(\pi)\cdot U(\tau)\cdot P_{-y_2}(\beta_2)\cdot G P_{x_2}(\beta_1)\cdot P_{x_{1,3}}(\eta)|\rho_B), \quad (15)$$

where $\beta_1 = \arccos(3/4)$ and $\beta_2 = \arccos(1/\sqrt{3})$. The free evolution time is $\tau = 1/4\,J$. The parameters required to obtain each of the possible states are given in Table II.

The basic blocks of the sequence are more clearly recognized in the representation shown in Table III. Here *X*, *Y*, and *Z* indicate the rotation direction of an rf pulse, the rotation

TABLE III. Pulse sequence for the preparation of the pseudopure states.

I_1	$\boldsymbol{X}, \boldsymbol{\eta}$	∇		U, τ	$-X, \pi$	U, τ	
I_2	X, β_1	∇	$-\boldsymbol{Y}, \beta_2$	U, τ	$-X, \pi$	U, τ	$\boldsymbol{Y}, \beta_2$
I_3	$\boldsymbol{X}, \boldsymbol{\eta}$	∇		U, τ	$-X, \pi$	U, τ	
I_1	∇	$\boldsymbol{Y}, \pi/4$	U, τ	$-\boldsymbol{X}, \pi$	$X, 3\pi/4$	∇	
I_2	∇		U, τ	$-X, \pi$		∇	
I_3	∇		U, τ	$-X, \pi$		∇	$\boldsymbol{Y}, \boldsymbol{\chi}$
I_1	U, τ	$-X, \pi$	U, τ	X, ξ_1	∇		
I_2	U, τ	$-X, \pi$	U, τ	X, ξ_2	∇		
I_3	U, τ	$-X, \pi$	U, τ	$\boldsymbol{X}, \boldsymbol{\xi}_3$	∇		

angle is given after the comma. "U, τ" indicates a period of free evolution for time τ, and ∇ means a gradient pulse. In all tables representing pulse sequences, pulses are applied starting in the upper left corner. They apply to the spins indicated on the left. The consecutive segments of the sequence are separated by the horizontal lines.

2. Tomography

Most terms of the density matrix—namely, all operator products—cannot be observed in NMR because their product with the measurement operator has a vanishing trace. Even under the conditions of fully resolved spin-spin interactions more commonly encountered in high-resolution NMR, full density matrix information is not available from simple NMR spectra. In our case, terms of the form $\mathbf{I}_{\alpha_i}\mathbf{I}_{\beta_j}$ and all higher-order products cannot be detected directly. Thus, as one can see from Eq. (8), much of the information in the density matrix is not accessible to direct measurement. Density matrix tomography is therefore mandatory to obtain this information. In high-resolution NMR part of the density matrix is visible already in the sign and phase of the NMR lines. It has been further shown that details of the density matrix can be extracted from two-dimensional spectroscopy [32]. In our situation, however, the spin interactions are not resolved and we must resort to alternative tomography concepts which will be applicable in the general case.

In this procedure, suitable pulse sequences are employed to convert the higher-order operator products to linear terms for detection. Two basic sequences were used for such conversions. These sequences are designed to convert the off-diagonal elements of the corresponding density matrix to observable operators. To summarize, only the $\mathbf{I}_{x_i}$ and $\mathbf{I}_{y_i}$ are accessible to direct measurement. $\mathbf{I}_{z_i}$ is readily converted to one of these through a simple $\pi/2$ pulse. $\mathbf{I}_{z_1}\mathbf{I}_{z_2}$ and $\mathbf{I}_{z_2}\mathbf{I}_{z_3}$ can be converted to $\mathbf{I}_{z_1}$ and $\mathbf{I}_{z_2}$, respectively, using variants of the sequence in Table VII(a) in the Appendix. $\mathbf{I}_{z_1}\mathbf{I}_{z_2}\mathbf{I}_{z_3}$ can be converted to $\mathbf{I}_{z_2}$ using the sequence in Table VII(b). $\mathbf{I}_{z_1}\mathbf{I}_{z_3}$ can be converted to $\mathbf{I}_{z_2}$ by applying both sequences successively. Product terms containing x and y components are readily converted to pure z-term products through simple selective pulses and are then accessible to tomography as above.

In order to account for losses due to relaxation and pulse errors, the losses were calibrated by applying two sequences of the same type consecutively and comparing the signal amplitudes before and after.

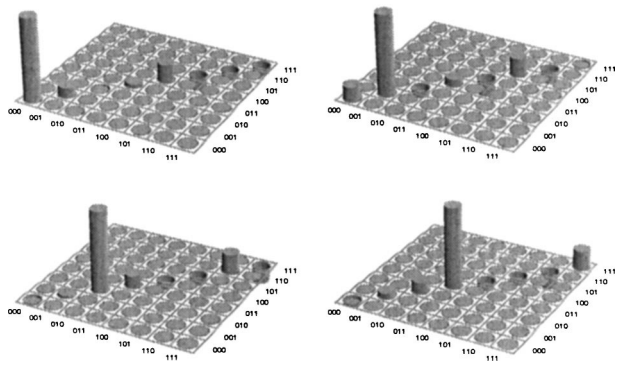

FIG. 3. Density matrix tomograms of the selected pseudopure states $\rho_{000}-\rho_{011}$.

3. Results

Using this preparation and tomography procedure, we prepared and measured the density matrices $\rho_{000}-\rho_{111}$. A selection ($\rho_{000}-\rho_{011}$) of the prepared states is shown in Fig. 3.

The density matrices clearly show deviations from the desired form. This can be attributed to nonuniform relaxation and different error sensitivity of the different elements of the density matrix. Since the preparation sequence employs gradient pulses and is, thus, essentially nonunitary ("lossy"), it is possible to improve on the overall result by adjusting suitable rotation angles and thus boosting appropriate relative amplitudes. The pulses within the preparation sequence which were chosen for such adjustments are highlighted in Table III. Using this procedure it was possible to obtain density matrices with a fidelity of $F>0.95$ for all eight pseudopure states where we have used the definition

$$F = 1 - \frac{1}{2}\mathrm{Tr}\{|\rho_{expt} - \rho_{theor}|^2\}. \tag{16}$$

The measured density matrices were normalized according to $\mathrm{Tr}\{\rho_{expt}\}=1$.

To demonstrate the achievable improvement, we juxtapose the two cases for ρ_{000} in Fig. 4.

V. IMPLEMENTATION OF THE COLLINS VERSION OF THE DEUTSCH-JOZSA ALGORITHM

A. Selection of oracles

The total number of functions is 2^{2^N} whereas the number of functions allowed for the Deutsch problem grows with the width N of the input as

$$\binom{2^N}{2^{N-1}} + 2. \tag{17}$$

Table IV shows a comparison of the statistics of the possible functions with the growing number of input bits. In the case of three bits, there are 72 functions of interest. Not all of them, however, are essentially different from the experimen-

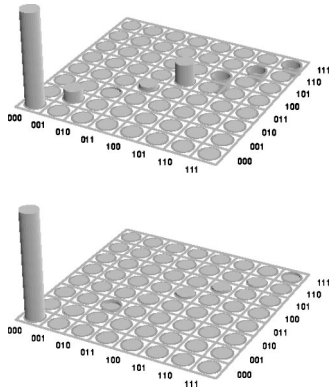

FIG. 4. Improvement of the fidelity of the preparation of a pseudopure state (ρ_{000}) achieved by accounting for the nonuniform relaxation of different density matrix components. Top: as prepared. Bottom: after refinement.

tal point of view. First, there is the freedom of reversing the states $|0\rangle$ and $|1\rangle$ to *spin up* and *spin down*, resulting in a mirror image function. This halves the number of functions. We present in Table V examples of some of constant and balanced oracle functions of the three-qubit CEMM Deutsch-Jozsa algorithm. The other constant function is of course like f_1 where all zeros are replaced by ones.

For further discussion, it is instructive to represent the oracles belonging to the remaining functions in the spin operator basis. It turns out that the oracles consist of linear combinations of certain sets of basis operators. There are seven such sets:

$$\mathbf{I}_0, \tag{18a}$$

$$\mathbf{I}_{z_1},$$

$$\mathbf{I}_{z_2}, \tag{18b}$$

$$\mathbf{I}_{z_3},$$

$$\mathbf{I}_{z_1}\mathbf{I}_{z_2},$$

$$\mathbf{I}_{z_1}\mathbf{I}_{z_3}, \tag{18c}$$

$$\mathbf{I}_{z_2}\mathbf{I}_{z_3},$$

$$\mathbf{I}_{z_1}\mathbf{I}_{z_2}\mathbf{I}_{z_3}, \tag{18d}$$

$$\mathbf{I}_{z_1}, \quad \mathbf{I}_{z_2}, \quad \mathbf{I}_{z_3}, \quad \mathbf{I}_{z_1}\mathbf{I}_{z_2}\mathbf{I}_{z_3}, \tag{18e}$$

TABLE IV. Statistics of the oracle functions of N qubits.

N	Total	Constant	Balanced	Rest
1	4	2	2	0
2	16	2	6	8
3	256	2	70	184

TABLE V. The 9 three-qubit oracle functions implemented here.

f	000	001	010	011	100	101	110	111
f_1	0	0	0	0	0	0	0	0
f_2	0	0	0	0	1	1	1	1
f_3	0	1	0	1	0	1	0	1
f_4	0	0	1	1	1	1	0	0
f_5	0	1	1	0	1	0	0	1
f_6	0	0	0	1	1	1	1	0
f_7	0	0	1	1	0	1	1	0
f_8	0	1	0	1	0	1	1	0
f_9	0	1	0	0	0	1	1	1

$$\mathbf{I}_{z_1}, \quad \mathbf{I}_{z_2}, \quad \mathbf{I}_{z_1}\mathbf{I}_{z_3}, \quad \mathbf{I}_{z_2}\mathbf{I}_{z_3},$$

$$\mathbf{I}_{z_1}, \quad \mathbf{I}_{z_3}, \quad \mathbf{I}_{z_1}\mathbf{I}_{z_2}, \quad \mathbf{I}_{z_3}\mathbf{I}_{z_2}, \tag{18f}$$

$$\mathbf{I}_{z_2}, \quad \mathbf{I}_{z_3}, \quad \mathbf{I}_{z_1}\mathbf{I}_{z_2}, \quad \mathbf{I}_{z_2}\mathbf{I}_{z_3},$$

$$\mathbf{I}_{z_1}, \quad \mathbf{I}_{z_1}\mathbf{I}_{z_2}, \quad \mathbf{I}_{z_1}\mathbf{I}_{z_3}, \quad \mathbf{I}_{z_1}\mathbf{I}_{z_2}\mathbf{I}_{z_3},$$

$$\mathbf{I}_{z_2}, \quad \mathbf{I}_{z_1}\mathbf{I}_{z_2}, \quad \mathbf{I}_{z_2}\mathbf{I}_{z_3}, \quad \mathbf{I}_{z_1}\mathbf{I}_{z_2}\mathbf{I}_{z_3}, \tag{18g}$$

$$\mathbf{I}_{z_3}, \quad \mathbf{I}_{z_1}\mathbf{I}_{z_3}, \quad \mathbf{I}_{z_2}\mathbf{I}_{z_3}, \quad \mathbf{I}_{z_1}\mathbf{I}_{z_2}\mathbf{I}_{z_3}.$$

Given the appropriate symmetry of the Hamiltonian, all oracles in a set can be mapped onto each other by exchanging the labels on two qubits. Thus, the implementation sequence for all oracles in a set is essentially the same. In principle, it would be sufficient to implement one oracle out of each of the seven sets. In this paper we adopt, for comparison, the choice of oracles made in [23]. These oracle functions correspond to the test functions listed in Table V.

Equations (19) show the unitary transforms associated with these oracle functions written partially as matrices as well as in the spin operator notation. The transforms U_1–U_5 involve only z Rotations (one-bit gates), transforms U_6 and U_8 involve effective two-bit gates, U_9 uses a three-bit gate, and U_7 needs a two-bit gate which is not directly available in our system due to the coupling network and must be implemented using next-neighbor interactions:

$$U_1 = \mathbf{I}_0, \tag{19a}$$

$$U_2 = \begin{pmatrix} +1 & 0 & 0 & 0 & 0 & 0 & 0 & 0 \\ 0 & +1 & 0 & 0 & 0 & 0 & 0 & 0 \\ 0 & 0 & +1 & 0 & 0 & 0 & 0 & 0 \\ 0 & 0 & 0 & +1 & 0 & 0 & 0 & 0 \\ 0 & 0 & 0 & 0 & -1 & 0 & 0 & 0 \\ 0 & 0 & 0 & 0 & 0 & -1 & 0 & 0 \\ 0 & 0 & 0 & 0 & 0 & 0 & -1 & 0 \\ 0 & 0 & 0 & 0 & 0 & 0 & 0 & -1 \end{pmatrix}$$

$$= 2\mathbf{I}_{z_1}, \tag{19b}$$

$$U_3 = 2\mathbf{I}_{z_3}, \tag{19c}$$

$$U_4 = 4\mathbf{I}_{z_1}\mathbf{I}_{z_2}, \tag{19d}$$

$$U_5 = 4\mathbf{I}_{z_1}\mathbf{I}_{z_2}\mathbf{I}_{z_3}, \tag{19e}$$

$$U_6 = \begin{pmatrix} +1 & 0 & 0 & 0 & 0 & 0 & 0 & 0 \\ 0 & +1 & 0 & 0 & 0 & 0 & 0 & 0 \\ 0 & 0 & +1 & 0 & 0 & 0 & 0 & 0 \\ 0 & 0 & 0 & -1 & 0 & 0 & 0 & 0 \\ 0 & 0 & 0 & 0 & -1 & 0 & 0 & 0 \\ 0 & 0 & 0 & 0 & 0 & -1 & 0 & 0 \\ 0 & 0 & 0 & 0 & 0 & 0 & -1 & 0 \\ 0 & 0 & 0 & 0 & 0 & 0 & 0 & +1 \end{pmatrix}$$
$$= \mathbf{I}_{z_1} + 2\mathbf{I}_{z_1}\mathbf{I}_{z_2} + 2\mathbf{I}_{z_1}\mathbf{I}_{z_3} - 4\mathbf{I}_{z_1}\mathbf{I}_{z_2}\mathbf{I}_{z_3}, \tag{19f}$$

$$U_7 = \mathbf{I}_{z_2} + 2\mathbf{I}_{z_1}\mathbf{I}_{z_2} + 2\mathbf{I}_{z_2}\mathbf{I}_{z_3} - 4\mathbf{I}_{z_1}\mathbf{I}_{z_2}\mathbf{I}_{z_3}, \tag{19g}$$

$$U_8 = \begin{pmatrix} +1 & 0 & 0 & 0 & 0 & 0 & 0 & 0 \\ 0 & -1 & 0 & 0 & 0 & 0 & 0 & 0 \\ 0 & 0 & +1 & 0 & 0 & 0 & 0 & 0 \\ 0 & 0 & 0 & -1 & 0 & 0 & 0 & 0 \\ 0 & 0 & 0 & 0 & +1 & 0 & 0 & 0 \\ 0 & 0 & 0 & 0 & 0 & -1 & 0 & 0 \\ 0 & 0 & 0 & 0 & 0 & 0 & -1 & 0 \\ 0 & 0 & 0 & 0 & 0 & 0 & 0 & +1 \end{pmatrix}$$
$$= \mathbf{I}_{z_3} + 2\mathbf{I}_{z_1}\mathbf{I}_{z_3} + 2\mathbf{I}_{z_2}\mathbf{I}_{z_3} - 4\mathbf{I}_{z_1}\mathbf{I}_{z_2}\mathbf{I}_{z_3}, \tag{19h}$$

$$U_9 = \mathbf{I}_{z_1} + \mathbf{I}_{z_3} - 2\mathbf{I}_{z_1}\mathbf{I}_{z_2} + 2\mathbf{I}_{z_2}\mathbf{I}_{z_3}. \tag{19i}$$

B. Entanglement, mixed vs pseudopure states

1. Entanglement

It has been shown [28] that entanglement between qubits does not always take place in the course of the Deutsch algorithm: some oracles are entangling in nature and others are not. Furthermore, entangling oracles only occur starting with at least three qubits. Here, we discuss the entangling nature of the oracles we implemented and contrast the expected results for the cases when the *Boltzmann* state is used as input instead of a *pseudopure* state.

It can be readily shown that applying the Deutsch algorithm to the pure (or pseudopure) state ρ_{000} in Eq. (8) will produce the following output density matrices for the first five oracles [Eqs. (20)]:

$$\rho_1 = \left(\frac{1}{2}\mathbf{I}_0 + \mathbf{I}_{z_1}\right)\left(\frac{1}{2}\mathbf{I}_0 + \mathbf{I}_{z_2}\right)\left(\frac{1}{2}\mathbf{I}_0 + \mathbf{I}_{z_3}\right), \tag{20a}$$

$$\rho_2 = \left(\frac{1}{2}\mathbf{I}_0 - \mathbf{I}_{z_1}\right)\left(\frac{1}{2}\mathbf{I}_0 + \mathbf{I}_{z_2}\right)\left(\frac{1}{2}\mathbf{I}_0 + \mathbf{I}_{z_3}\right), \tag{20b}$$

$$\rho_3 = \left(\frac{1}{2}\mathbf{I}_0 + \mathbf{I}_{z_1}\right)\left(\frac{1}{2}\mathbf{I}_0 + \mathbf{I}_{z_2}\right)\left(\frac{1}{2}\mathbf{I}_0 - \mathbf{I}_{z_3}\right), \tag{20c}$$

$$\rho_4 = \left(\frac{1}{2}\mathbf{I}_0 - \mathbf{I}_{z_1}\right)\left(\frac{1}{2}\mathbf{I}_0 - \mathbf{I}_{z_2}\right)\left(\frac{1}{2}\mathbf{I}_0 + \mathbf{I}_{z_3}\right), \tag{20d}$$

$$\rho_5 = \left(\frac{1}{2}\mathbf{I}_0 - \mathbf{I}_{z_1}\right)\left(\frac{1}{2}\mathbf{I}_0 - \mathbf{I}_{z_2}\right)\left(\frac{1}{2}\mathbf{I}_0 - \mathbf{I}_{z_3}\right). \tag{20e}$$

These are clearly fully separable states, so, at least in the final state, no entanglement is present.

Oracles 6–9 [Eqs. (21)] produce entangled density matrices. This is most clearly demonstrated by rotating the output states into one of the base vectors of an entangled basis by means of local transformations. This is summarized in the following equations:

$$P_{y_2}\left(-\frac{\pi}{2}\right)\rho_6 = \left(\frac{1}{2}\mathbf{I}_0 - \mathbf{I}_{z_1}\right)\left(\frac{1}{4}\mathbf{I}_0 + \mathbf{I}_{x_2}\mathbf{I}_{x_3} + \mathbf{I}_{y_2}\mathbf{I}_{y_3} - \mathbf{I}_{z_2}\mathbf{I}_{z_3}\right)$$
$$= \begin{pmatrix} 0 & 0 \\ 0 & 1 \end{pmatrix} \otimes \begin{pmatrix} 0 & 0 & 0 & 0 \\ 0 & \frac{1}{2} & \frac{1}{2} & 0 \\ 0 & \frac{1}{2} & \frac{1}{2} & 0 \\ 0 & 0 & 0 & 0 \end{pmatrix}, \tag{21a}$$

$$P_{y_3}\left(-\frac{\pi}{2}\right)\rho_7 = \left(\frac{1}{2}\mathbf{I}_0 - \mathbf{I}_{z_2}\right)\left(\frac{1}{4}\mathbf{I}_0 + \mathbf{I}_{x_1}\mathbf{I}_{x_3} + \mathbf{I}_{y_1}\mathbf{I}_{y_3} - \mathbf{I}_{z_1}\mathbf{I}_{z_3}\right), \tag{21b}$$

$$P_{y_3}\left(-\frac{\pi}{2}\right)\rho_8 = \left(\frac{1}{2}\mathbf{I}_0 - \mathbf{I}_{z_3}\right)\left(\frac{1}{4}\mathbf{I}_0 + \mathbf{I}_{x_1}\mathbf{I}_{x_2} + \mathbf{I}_{y_1}\mathbf{I}_{y_2} - \mathbf{I}_{z_1}\mathbf{I}_{z_2}\right), \tag{21c}$$

$$P_{y_1}(\pi)P_{y_2}\left(-\frac{\pi}{2}\right)\rho_9 = \frac{1}{8}\mathbf{I}_0 + \frac{1}{2}(\mathbf{I}_{z_1}\mathbf{I}_{z_2} + \mathbf{I}_{z_2}\mathbf{I}_{z_3} + \mathbf{I}_{z_1}\mathbf{I}_{z_3})$$
$$+ \mathbf{I}_{x_1}\mathbf{I}_{x_2}\mathbf{I}_{x_3} - \mathbf{I}_{x_1}\mathbf{I}_{y_2}\mathbf{I}_{y_3} - \mathbf{I}_{y_1}\mathbf{I}_{x_2}\mathbf{I}_{y_3}$$
$$- \mathbf{I}_{y_1}\mathbf{I}_{y_2}\mathbf{I}_{x_3}$$
$$= \begin{pmatrix} \frac{1}{2} & 0 & 0 & 0 & 0 & 0 & 0 & \frac{1}{2} \\ 0 & 0 & 0 & 0 & 0 & 0 & 0 & 0 \\ 0 & 0 & 0 & 0 & 0 & 0 & 0 & 0 \\ 0 & 0 & 0 & 0 & 0 & 0 & 0 & 0 \\ 0 & 0 & 0 & 0 & 0 & 0 & 0 & 0 \\ 0 & 0 & 0 & 0 & 0 & 0 & 0 & 0 \\ 0 & 0 & 0 & 0 & 0 & 0 & 0 & 0 \\ \frac{1}{2} & 0 & 0 & 0 & 0 & 0 & 0 & \frac{1}{2} \end{pmatrix}. \tag{21d}$$

TABLE VI. Fidelity and decision parameter for the experimental implementation of the DJ algorithm.

	ρ_1	ρ_2	ρ_3	ρ_4	ρ_5	ρ_6	ρ_7	ρ_8	ρ_9
D	0.862	0.206	0.121	0.051	−0.066	0.084	0.015	0.027	0.184
F	0.862	0.874	0.879	0.897	0.905	0.891	0.819	0.862	0.646

Up to a local (confined to one qubit) transformation, the output states for the oracles U_6–U_8 correspond to a product of a one-qubit state $|1\rangle$ and the *Bell state* $\Psi^+=1/\sqrt{2}(|01\rangle+|10\rangle)$. The state produced by U_9 can be locally transformed to the *GHZ state* $1/\sqrt{2}(|000\rangle+|111\rangle)$.

2. Input density matrix: Pseudopure vs Boltzmann

The final states shown in Eqs. (21) are only produced if the pseudopure state ρ_{000} from Eq. (8) is used as input to the algorithm. If one starts, instead, from the Boltzmann state, like in [23], the final density matrices do not reflect entanglement in any case. We therefore note that our final density matrices of the DJ algorithm as presented in Figs. 7–9 do represent the expected entanglement produced by the oracles U_6 and U_8.

C. Implementation of oracle functions

The pulse sequences required for the implementation of these transforms are as follows. U_1 is the identity transform and requires no pulses. U_2 and U_3 are implemented by applying a π pulse to the first and third spins, respectively. U_4 and U_5 require a π rotation of spins 1 and 2 and 1, 2, and 3, respectively. The other four sequences require two- and three-qubit gates. They are shown in the Appendix.

After applying the different pulse sequences corresponding to the nine different oracle functions we have evaluated the decision parameter D—namely, the population of the state $|000\rangle\langle 000|$ which according to the DJ algorithm should be either 1 for the constant functions or 0 for balanced functions together with the fidelity F as defined in Eq. (16). Fidelities and the decision parameter for the experimental results on the Deutsch algorithm are shown in Table VI.

D. Output tomography

The DJ algorithm does not require full knowledge of the resulting density matrix for the evaluation of the decision criterion. It is, therefore, common to present just some spectral signatures which are consistent with the expected outcome of the algorithm. However, in order to evaluate the performance of the implementation of the algorithm it is necessary to perform a complete tomography of the resulting density matrix. We have done this for all nine oracle functions and present some of the results in the following.

For all density matrices, one expects a vanishing imaginary part; however, small imaginary contributions were detected experimentally. In the following graphical representations of the density matrices, we only display the real part. The imaginary part was considered when calculating the fidelities reported.

We start with the identity operation U_1 which represents the only constant function. Although this corresponds to "no operation" we have implemented it with a similar pulse sequence as all the others except for phase settings such that no effective operation occurs in the ideal situation. Figure 5 shows the comparison between the expected and measured results for the oracle function f_1. The deviations from the ideal situation are due to pulse imperfections during preparation and tomography. Since this is an identity transformation, it is suitable for the assessment of the fidelity of the preparation and the tomography procedures.

Figure 6 shows the comparison between the expected and measured results for the oracle function f_2. The corresponding unitary transformation involves only a spin-1 z rotation. Note that f_2 is a balanced function and correspondingly the population of the state $|000\rangle\langle 000|$ is close to zero like for all the other balanced function.

The next two functions f_6 (Fig. 7) and f_8 (Fig. 8) involve two-spin and three-spin gates. In the course of the quantum algorithm the corresponding unitary transformations generate entangled states, as described in Sec. V B 1. To emphasize the Bell-like entangled structure of the obtained density matrix, we subjected the data for U_6 to a local transform according to

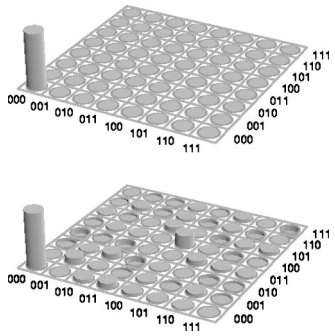

FIG. 5. Comparison between the theoretically expected (top) and experimentally obtained (bottom) output density matrix for the Cleve-Deutsch-Jozsa algorithm (U_1).

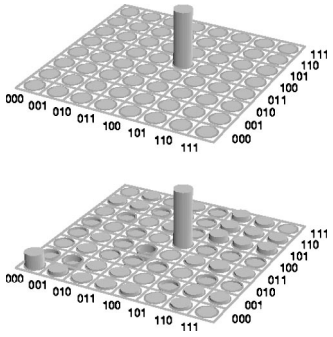

FIG. 6. Comparison between the theoretically expected (top) and experimentally obtained (bottom) output density matrix for the Cleve-Deutsch-Jozsa algorithm (U_2).

$$P_{x_3}(\pi)P_{y_2}\left(-\frac{\pi}{2}\right)\rho_6 = \left(\frac{1}{2}\mathbf{I}_0 - \mathbf{I}_{z_1}\right)\left(\frac{1}{4}\mathbf{I}_0 + \mathbf{I}_{x_2}\mathbf{I}_{x_3} + \mathbf{I}_{y_2}\mathbf{I}_{y_3} + \mathbf{I}_{z_2}\mathbf{I}_{z_3}\right) = \begin{pmatrix} 0 & 0 \\ 0 & 1 \end{pmatrix} \otimes \begin{pmatrix} \frac{1}{2} & 0 & 0 & \frac{1}{2} \\ 0 & 0 & 0 & 0 \\ 0 & 0 & 0 & 0 \\ \frac{1}{2} & 0 & 0 & \frac{1}{2} \end{pmatrix} \tag{22}$$

to obtain the Bell Φ^+ state which is more suitable for graphical representation. Figure 9 shows a comparison between the theoretically expected and experimentally obtained density matrices.

VI. SUMMARY

We have implemented the CEMM version of the Deutsch-Jozsa algorithm for three qubits with three ^{19}F nuclear spins in trifluoroaniline by applying liquid-state NMR. As an extension of earlier work [23] we have started from pseudopure

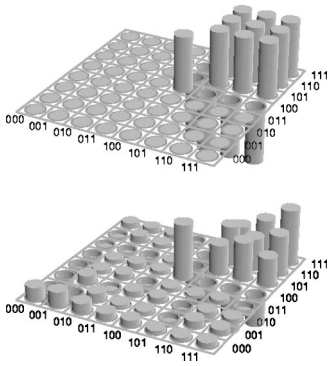

FIG. 7. Comparison between the theoretically expected (top) and experimentally obtained (bottom) output density matrix for the Cleve-Deutsch-Jozsa algorithm (U_6).

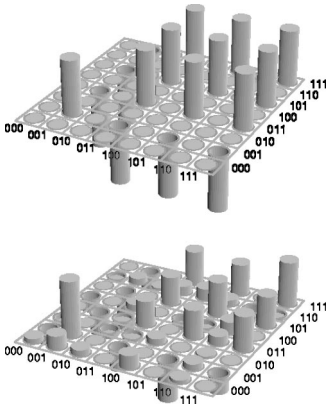

FIG. 8. Comparison between the theoretically expected (top) and experimentally obtained (bottom) output density matrix for the Cleve-Deutsch-Jozsa algorithm (U_8).

density matrices as initial states and have performed extensive density matrix tomography of the final density matrices. This allowed us to verify the performance of the experimental implementation and on the other hand to investigate the type of entanglement involved in some of the oracle functions. Moreover, the type of our implementation and tomography can be considered a template for the general case encountered usually in solids and other systems where the spin interactions are not resolved and only spin—but not transition-selective irradiation—can be performed.

ACKNOWLEDGMENTS

We would like to thank Dr. S. Krämer for active cooperation, the members of the "Landesswerpunkt Quanten-Informationsverarbeitung" for collaboration, and the Landesstiftung Baden-Württemberg for financial support.

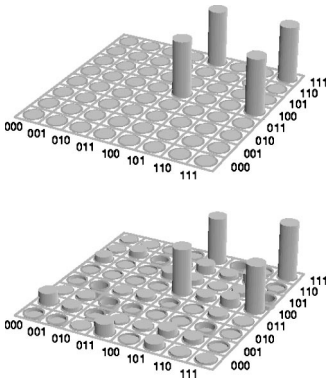

FIG. 9. Output density matrix for the oracle U_6 after a local rotation onto the Bell state Φ^+ in the subspace of spins 2 and 3.

APPENDIX: PULSE SEQUENCES

For completeness, we list the pulse sequences used for density matrix tomography and implementation of the oracle functions in Tables VII–IX. The following notation is used: X, Y, and Z indicate the rotation direction of an rf pulse; the rotation angle is given after the comma. "U,τ" indicates a period of free evolution for time τ, and ∇ means a gradient pulse. In all tables representing pulse sequences, pulses are applied starting in the upper left corner. They apply to the spins indicated on the left. Consecutive segments of the sequence are separated by horizontal lines.

The pulse sequence for the oracle U_7 needs to be rather long because there is no sufficient direct coupling between spins 1 and 3 so that next-neighbor couplings must be used instead.

TABLE VII. Pulse sequences used for density matrix tomography: (a) conversion of the term $\mathbf{I}_{z_1}\mathbf{I}_{z_2}$ to $\mathbf{I}_{z_1}$, (b) conversion of the term $\mathbf{I}_{z_1}\mathbf{I}_{z_2}\mathbf{I}_{z_3}$ to $\mathbf{I}_{z_2}$.

			(a)			
I_1	$Y,\ \pi/2$	$U,\ 1/4J$	$X,\ \pi$	$U,\ 1/4J$	$-X,\ \pi/2$	∇
I_2		$U,\ 1/4J$	$X,\ \pi$	$U,\ 1/4J$		∇
I_3		$U,\ 1/4J$		$U,\ 1/4J$		∇
			(b)			
I_1		$U,\ 1/4J$	$X,\ \pi$	$U,\ 1/4J$		∇
I_2	$Y,\ \pi/2$	$U,\ 1/4J$	$X,\ \pi$	$U,\ 1/4J$	$-Y,\ \pi/2$	∇
I_3		$U,\ 1/4J$	$X,\ \pi$	$U,\ 1/4J$		∇

TABLE VIII. Pulse sequence implementing the oracles U_6 and U_7 of the Deutsch-Jozsa algorithm.

				U_6			
I_1		$U,\ 1/4J$	$X,\ \pi$	$U,\ 1/4J$		∇	
I_2	$Y,\ \pi/2$	$U,\ 1/4J$	$X,\ \pi$	$U,\ 1/4J$	$-Y,\ \pi/2$	∇	
I_3		$U,\ 1/4J$	$X,\ \pi$	$U,\ 1/4J$		∇	
				U_7			
I_1	$-Z,\ \pi/2$	$U,\ 1/8J$		$U,\ 1/8J$	$X,\ \pi$	$U,\ 1/8J$	
I_2	$Z,\ \pi$	$U,\ 1/8J$		$U,\ 1/8J$	$X,\ \pi$	$U,\ 1/8J$	
I_3	$-Z,\ \pi/2$	$U,\ 1/8J$	$X,\ \pi$	$U,\ 1/8J$		$U,\ 1/8J$	$-X,\ \pi$
I_1	$U,\ 1/8J$	$-X,\ \pi$		$U,\ 1/8J$	$X,\ \pi$	$U,\ 1/8J$	
I_2	$U,\ 1/8J$	$Y,\ \pi/2$	$Z,\ \pi$	$U,\ 1/8J$		$U,\ 1/8J$	$X,\ \pi$
I_3	$U,\ 1/8J$			$U,\ 1/8J$		$U,\ 1/8J$	$X,\ \pi$
I_1	$U,\ 1/8J$	$-X,\ \pi$	$U,\ 1/8J$		$U,\ 1/8J$		$U,\ 1/8J$
I_2	$U,\ 1/8J$		$U,\ 1/8J$	$-X,\ \pi/2$	$U,\ 1/8J$		$U,\ 1/8J$
I_3	$U,\ 1/8J$		$U,\ 1/8J$	$-X,\ \pi$	$U,\ 1/8J$	$X,\ \pi$	$U,\ 1/8J$
I_1	$X,\ \pi$	$U,\ 1/8J$		$U,\ 1/8J$	$-X,\ \pi$	$U,\ 1/8J$	$X,\ \pi$
I_2	$X,\ \pi$	$U,\ 1/8J$		$U,\ 1/8J$	$Y,\ \pi/2$	$U,\ 1/8J$	
I_3		$U,\ 1/8J$	$-X,\ \pi$	$U,\ 1/8J$		$U,\ 1/8J$	
I_1	$U,\ 1/8J$		$U,\ 1/8J$	$-X,\ \pi$	$U,\ 1/8J$		$-Z,\ \pi/2$
I_2	$U,\ 1/8J$	$X,\ \pi$	$U,\ 1/8J$		$U,\ 1/8J$	$-X,\ \pi/2$	
I_3	$U,\ 1/8J$	$X,\ \pi$	$U,\ 1/8J$		$U,\ 1/8J$	$-X,\ \pi$	$Z,\ \pi/2$

TABLE IX. Pulse sequence implementing the oracles U_8 and U_9 of the Deutsch-Jozsa algorithm.

				U_8			
I_1	$-Z,\ \pi/2$	$U,\ 1/8J$		$U,\ 1/8J$	$X,\ \pi$	$U,\ 1/8J$	
I_2	$-Z,\ \pi/2$	$U,\ 1/8J$		$U,\ 1/8J$	$X,\ \pi$	$U,\ 1/8J$	
I_3	$Z,\ \pi$	$U,\ 1/8J$	$X,\ \pi$	$U,\ 1/8J$		$U,\ 1/8J$	$-X,\ \pi$
I_1	$U,\ 1/8J$	$-X,\ \pi$					
I_2	$U,\ 1/8J$	$-X,\ \pi$					
I_3	$U,\ 1/8J$						
				U_9			
I_1	$-Z,\ \pi/2$	$Y,\ \pi$	$U,\ 1/8J$	$X,\ \pi$	$U,\ 1/8J$		
I_2			$U,\ 1/8J$	$X,\ \pi$	$U,\ 1/8J$	$-X,\ \pi$	
I_3	$Z,\ \pi/2$		$U,\ 1/8J$	$X,\ \pi$	$U,\ 1/8J$	$-X,\ \pi$	

[1] D. Deutsch, Proc. R. Soc. London, Ser. A **400**, 97 (1985).
[2] D. Deutsch and R. Jozsa, Proc. R. Soc. London, Ser. A **439**, 553 (1992).
[3] C. H. Bennett, G. Brassard, C. Crépeau, R. Jozsa, A. Peres, and W. K. Wootters, Phys. Rev. Lett. **70**, 1895 (1993).
[4] P. W. Shor, Phys. Rev. A **52**, R2493 (1995).
[5] J. I. Cirac and P. Zoller, Phys. Rev. Lett. **74**, 4091 (1995).
[6] C. Monroe, D. M. Meekhof, B. E. King, W. M. Itano, and D. J. Wineland, Phys. Rev. Lett. **75**, 4714 (1995).
[7] A. M. Steane, Phys. Rev. Lett. **77**, 793 (1996).
[8] L. K. Grover, Phys. Rev. Lett. **79**, 325 (1997).
[9] D. Bouwmeester, J.-W. Pan, K. Mattle, M. Eibl, H. Weinfurter, and A. Zeilinger, Nature (London) **390**, 575 (1997).
[10] B. E. Kane, Nature (London) **393**, 133 (1998).
[11] A. Shnirman, G. Schön, and Z. Hermon, Phys. Rev. Lett. **79**, 2371 (1997).
[12] Y. Nakamura, Y. A. Pashkin, and J. S. Tsai, Nature (London) **398**, 786 (1999).
[13] E. Knill, R. Laflamme, and G. J. Milburn, Nature (London) **409**, 46 (2001).
[14] D. G. Cory, A. F. Fahmy, and T. F. Havel, Proc. Natl. Acad. Sci. U.S.A. **94**, 1634 (1997).
[15] D. G. Cory, M. D. Price, and T. F. Havel, Physica D **120**, 82 (1998).
[16] N. A. Gershenfeld and I. L. Chuang, Science **275**, 350 (1997).
[17] W. S. Warren, N. Gershenfeld, and I. Chuang, Science **277**, 1688 (1997).
[18] E. Knill, I. Chuang, and R. Laflamme, Phys. Rev. A **57**, 3348 (1998).
[19] J. A. Jones and M. Mosca, J. Chem. Phys. **109**, 1648 (1998).
[20] R. Laflamme, E. Knill, W. H. Zurek, P. Catasti, and S. V. S. Mariappan, Philos. Trans. R. Soc. London, Ser. A **356**, 1941 (1998).
[21] K. Dorai, Arvind, and A. Kumar, Phys. Rev. A **61**, 042306/1 (2000).
[22] L. M. K. Vandersypen, M. Steffen, G. Breyta, C. S. Yannoni, M. H. Sherwood, and I. L. Chuang, Nature (London) **414**, 883 (2001).
[23] Arvind, K. Dorai, and A. Kumar, Pramana, J. Phys. **56**, L705 (2001).
[24] N. Boulant, E. M. Fortunato, M. A. Pravia, G. Teklemariam, D. G. Cory, and T. F. Havel, Phys. Rev. A **65**, 024302 (2002).
[25] G. Teklemariam, E. M. Fortunato, M. A. Pravia, Y. Sharf, T. F. Havel, D. G. Cory, A. Bhattaharyya, and J. Hou, Phys. Rev. A **66**, 012309 (2002).
[26] S. Guide, M. Riebe, G. P. T. Lancaster, C. Becher, J. Eschner, H. Haffner, F. Schmidt-Kaler, I. L. Chuang, and R. Blatt, Nature (London) **421**, 48 (2003).
[27] I. L. Chuang, L. M. K. Vandersypen, X. Zhou, D. W. Leung, and S. Lloyd, Nature (London) **393**, 143 (1998).
[28] D. Collins, K. W. Kim, and W. C. Holton, Phys. Rev. A **58**, R1633 (1998).
[29] R. Cleve, A. Ekert, C. Macchiavello, and M. Mosca, Proc. R. Soc. London, Ser. A **454**, 339 (1998).
[30] O. Mangold, Master's thesis, Universität Stuttgart, 2003.
[31] M. Mehring, *Principles of High Resolution NMR in Solids*, 2nd ed. (Springer, Berlin, 1983).
[32] Z. L. Mádi, R. Brüschweiler, and R. R. Ernst, J. Chem. Phys. **109**, 10 603 (1998).